

1 **EVALUATION OF ICHNODIVERSITY BY IMAGE-RESAMPLING METHOD TO**
2 **CORRECT OUTCROP EXPOSURE BIAS**

3 KAZUKI KIKUCHI¹, HAJIME NARUSE¹, and NOBUHIRO KOTAKE²

4 *¹Department of Geology and Mineralogy, Graduate School of Science, Kyoto University,*
5 *Kitashirakawaoiwake-cho, Sakyo-ku, Kyoto, 606-8502, Japan*

6 *²Department of Earth Sciences, Graduate School of Science, Chiba University, 1-33,*
7 *Yayoi-cho, Inage-ku, Chiba, 263-8522, Japan*

8 *email: kikuchi@kueps.kyoto-u.ac.jp*

9 *RRH: NEW EVALUATION METHOD OF ICHNODIVERSITY*

10 *LRH: K. KIKUCHI ET AL.*

11 **ABSTRACT**

12 **We propose a new method to evaluate the diversity of ichnofossils from**
13 **outcrop. Ichnodiversity (defined here as the number of ichnotaxa) characterizes**
14 **paleoenvironmental conditions. However, the apparent numbers of ichnotaxa**
15 **observed in outcrops are significantly affected by differences in areas of exposed**
16 **outcrops. This study proposes a new method to evaluate ichnodiversity, independent of**
17 **outcrop exposure bias, by using an image-resampling technique combined with the**
18 **shareholder quorum subsampling method. In this method, the relationship between**
19 **observed and detected numbers of ichnotaxa is estimated by subsampling from**
20 **existing outcrop images. The relative diversity of ichnotaxa is obtained at a given**
21 **value of the estimated coverage parameter, representing the ratio of the observed**
22 **number of ichnotaxa to the actual diversity. The method was verified by analyzing**
23 **artificial images of ichnoassemblages, and the method successfully estimated**
24 **reasonable values of relative diversity of ichnotaxa. It was also suggested that the**
25 **spatial distribution patterns of ichnofossils on the bedding planes does not affect the**
26 **estimated intensity of ichnodiversity when using this method. This method was also**
27 **applied to field data pertaining to deposits of the submarine channel-levee complex in**
28 **the Oligocene Izaki Olistolith of the Nichinan Group, southwest Japan. As a result, the**
29 **ichnodiversity of the successions in the Izaki Olistolith was reconstructed to be**
30 **relatively high in channel deposits and low in levee deposits.**

31
32 **INTRODUCTION**

33 Ichnofossils represent a record of the response of ancient benthic animals to
34 changes in environmental conditions. Therefore, ichnological data are important for
35 assessing sedimentary environments of the sea floor and also to understand the ethology of
36 ancient benthic animals.

37 Ichnodiversity, which is regarded as the number of ichnotaxa at the ichnogenus
38 level, is an important and useful parameter for evaluating sedimentary environments of the
39 seafloor. Many studies have assessed not only the physicochemical disturbances including
40 sedimentation rate, energy level, sediment properties, salinity, and pore water oxygenation
41 (Bromley and Ekdale 1984; Buatois et al. 1997; Knaust 2007; Heard and Pickering 2008;
42 Hauck et al. 2009; Cummings and Hodgson 2011; Gingras et al. 2011; Phillips et al. 2011;
43 Callow et al. 2013; Heard et al. 2014; Bayet-Goll et al. 2015; Timmer et al. 2016), but also
44 biological factors such as organic matter input (Pearson and Rosenberg 1978; Wetzel and
45 Uchman 1998; Hyland et al. 2005; Callow et al. 2014). In addition, ichnodiversity is
46 strongly controlled by differences in sedimentary facies: the diversity of ichnotaxa found in
47 the submarine channel facies seems to be lower than that in the levee facies (Heard and
48 Pickering 2008; Cummings and Hodgson 2011; Phillips et al. 2011; Callow et al. 2013;
49 Heard et al. 2014). Furthermore, ichnodiversity can also provide informative data for the
50 evolutionary history of ethological strategies of benthic communities (Uchman 2003;
51 Buatois et al. 2016).

52 Previous studies have discussed ichnodiversity based on qualitative data using the
53 apparent number of ichnotaxa at the ichnogenus level obtained from outcrop observations
54 (Buatois and Mángano 2013). The apparent numbers of ichnotaxa strongly reflect not only

55 the actual diversity in activities of benthic animals, but also exposed areas of observed
56 outcrops (Orr 2001). In the case of outcrop observation, the numbers of ichnotaxa must be
57 simply increased by increasing the area of the observed bedding plane. The observational
58 biases mentioned above can be treated as types of sample size effects. Thus, quantitative
59 approaches are required for evaluation of ichnodiversity (Buatois et al. 2016).

60 Several established methods are available for correcting sample size effects in
61 studies of ecology and paleobiology. For instance, the rarefaction method (Sanders 1968) is
62 a traditional method to compare biodiversity among assemblages with respective sample
63 sizes. In this method, rarefaction curves for each assemblage, which show relationships
64 between sample size and expected species richness, are described to standardize diversity at
65 a given sample size (e.g., Hurlbert 1971). This method is suitable when size of collected
66 samples is significantly large and the diversity of communities is relatively low (Alroy
67 2010c; Chao and Jost 2012). However, this method tends to underestimate biodiversity,
68 especially in highly diverse communities because estimated biodiversity standardized by
69 sample size strongly depends on species-abundance distributions of the real communities
70 (Alroy 2010c; Chao and Jost 2012). The estimated biodiversity of a community with a
71 small number of taxa can be saturated at relatively small sample sizes, but this is not
72 adequate for a highly diverse community. Therefore, comparison of biodiversity based on
73 the sample size is not usually “fair” because the sample diversity of one community might
74 cover nearly all of the real diversity, whereas the sample diversity of the other community
75 might represent only a part of the real diversity (Chao and Jost 2012). Recently, Alroy
76 (2010b, 2010c) proposed the shareholder quorum subsampling (SQS) method to solve this

77 problem. In this method, the biodiversity of communities are compared with each other at
78 the same value of the sample coverage parameter, which represents the sum of frequencies
79 of each taxon included in hypothetical populations (Alroy 2010a, 2010b, 2010c; Chao and
80 Jost 2012). The sample coverage is estimated by Good-Turing frequency estimation (Good
81 1953) or the slope of the tangential lines of the rarefaction curves (Chao and Jost 2012).
82 Even though the species richness value estimated by the SQS method is always lower than
83 the real diversity, the ratio of species richness values between any two samples is expected
84 to match the ratio of the real diversity of those communities. Thus, the SQS method can be
85 used for estimating relative variation of biodiversity.

86 Ichnodiversity, however, cannot be analyzed by established methods for
87 biodiversity described above. Although these methods require the number of individuals of
88 each taxon for obtaining rarefaction curves or values of sample coverage, it is difficult to
89 count the number of individuals of ichnofossils because of their morphological
90 characteristics. The apparent number of ichnofossil specimens strongly depends on their
91 structural organization. Ichnofossils that appear as discrete scattered spots are counted as
92 large numbers, whereas those which make connected networks appear as a single specimen,
93 even though they are extremely large in size. For example, planar-formed, regular network
94 graphoglyptids such as *Megagraption* or *Paleodictyon* may be preserved as multiple spots
95 on the bottom of a single sandstone bed. However, it is almost impossible to judge if
96 multiple spots on a bedding plane actually represent multiple individuals or fragments of a
97 single specimen. Even if there is intact preservation, it is difficult to recognize a single
98 individual from planar-formed ichnofossils that occupy very large areas of the bedding

99 plane because the exposed region of the ichnofossil may represent only a part of the entire
100 morphology of an individual specimen.

101 In previous studies dealing with ichnodiversity, most authors attempted to
102 attenuate the effect of the outcrop exposure and observe the bedding plane as large as
103 possible (e.g., Heard and Pickering 2008; Cummings and Hodgson 2011). In this approach,
104 there is no criterion to judge if the area of observed outcrops is adequate for fair evaluation
105 of ichnodiversity. Recently, three different methods were applied for evaluating
106 ichnodiversity: the rarefaction method (Buatois et al. 2016), the ichnoabundance method
107 (Knaust et al. 2014), and the Gini Index method (Gianetti and McCann 2010). These
108 methods require the relative abundance of each ichnotaxon, which was estimated from the
109 numbers reported previously (Buatois et al. 2016) or apparent numbers of sections of
110 tubular structures on the bedding planes. However, as mentioned above, these
111 methodologies are not suitable for estimating the abundance of ichnofossils at outcrop scale.
112 In addition, the two methods described above are known to be problematic for estimation of
113 biodiversity (Alroy 2010c; Chao and Jost 2012). Thus, methods for assessing ichnofossil
114 diversity are not yet well established.

115 We propose a new method to evaluate ichnodiversity, independent of exposed area
116 of outcrops, by using an image-resampling technique with the application of the SQS
117 method. This method is applicable to images such as vertical successions, top or bottom
118 surfaces of beds, or polished sections of sedimentary rocks. In this method, (1) the
119 relationship between observed and detected numbers of ichnotaxa is obtained by
120 subsampling from existing outcrop or polished section images; (2) the coverage parameter

121 of the sampled number of ichnotaxa and real ichnodiversity is then estimated from the fit
122 curve of subsampled data; and (3) the sample diversity of ichnotaxa is calculated from a
123 given value of the coverage parameter. We verified the method by applying it to artificial
124 data of ichnoassemblages. In this test, effects of variation on distribution patterns of
125 ichnofossils on bedding planes and shortage of outcrop exposure areas were examined.
126 Finally, we applied the new method to field data obtained from the Oligocene submarine
127 channel-levee complex to provide the first example of ichnological data independent of
128 outcrop exposure bias.

129

130 METHODOLOGY OF IMAGE-RESAMPLING

131 We named this method “Measurement of Ichnofossil Diversity by
132 Image-Resampling Technique” (MIDIRT) (Fig. 1). The step-wise procedure of this method
133 is listed below.

134

135

136 1. Image Acquisition

137 First, outcrop photographs are taken in the field or laboratory. The photographs should be
138 taken at random and perpendicular to the outcrop surfaces containing ichnofossils.

139 Ichnofossils may be observable on various types of surfaces, such as bottom surfaces of
140 sandstone beds or polished sections. This methodology is applicable for any type of surface,
141 but only photographs of the same type of surface can be compared with each other.

142 Additionally, photographs should not be taken to preferentially show specific ichnotaxa.

143

144

2. Identification of Ichnotaxa

145

146

147

148

149

150

3. Image Resampling

151

152

153

154

155

156

157

158

159

160

161

4. Curve Fitting to Resampled Data

162

163

164

Each ichnotaxon is identified from the acquired outcrop images. The regions of ichnofossils in images are colored with a specific grayscale or RGB color value for each ichnotaxon, and regions where ichnofossils are absent are colored white. Regions outside the outcrop surfaces are colored black.

The line-of-interest in data resampling is randomly set in the acquired outcrop image. If the resampling line protrudes from the outcrop, the line turns up to the next row of pixels. The number of ichnotaxa on the line is then counted. As the length of the resampling line (L) increases, the number of counted ichnotaxa (N_{is}) is expected to increase. The length of the resampling line (L) ranges from one to the maximum value of outcrop area. For each length, the resampling process is repeated 100 times, and then the mean value of N_{is} ($\overline{N_{is}}$), is regarded as the representative value of the resampled data at the given resampling length. This value shows the expected number of ichnotaxa when the outcrop is explored by the resampling line that is L in length.

Repetition of the resampling process provides the relationship between the observed length and number of ichnotaxa. Alroy (2010b, 2010c) attempted to estimate the sample coverage, which was expressed by the sum of the frequencies of taxa that

165 hypothetical populations included, from chances of occurrence of undiscovered taxa using
166 Good-Turing estimation (Good 1953). This implies that the completeness of the sample
167 (sample coverage) can be evaluated by differences between unity and chance of occurrence
168 of undiscovered taxa. Although the chance of occurrence of undiscovered taxa cannot be
169 directly measured, the ratio of the number of singletons in the sample when the relative
170 frequencies of each taxon are based on a binomial distribution can be approximated. In
171 addition, Chao and Jost (2012) indicated that sample coverage for biodiversity is equal to
172 the slope of the tangential line of rarefaction curves in that condition. For the analytical
173 calculation of the slope of tangential lines as an estimator of the chance of occurrence of
174 undiscovered taxa, we employed a fitting function to the resampled data. The chance of
175 occurrence of undiscovered taxa can be estimated from using differential calculus of the
176 fitting function. Although the observed number of ichnotaxa (\overline{N}_{is}) increases as the
177 resampling length (L) increases, the increasing rate of \overline{N}_{is} is expected to decline
178 gradually. Therefore, we employed the following as the fitting function (Mauffrey et al.
179 2007):

$$180 \quad E_s = a_1 \ln(1 + a_2 L) \quad (1)$$

181 where E_s denotes the expected number of ichnotaxa and a_1 and a_2 are fitting
182 coefficients. The parameter a_1 is a dimensionless variable, and a_2 denotes a coefficient
183 for describing an increase rate of observed numbers of ichnotaxa, which has a dimension of
184 the inverse number of the length scale. The obtained curve of Equation 1 can be regarded as
185 the equivalent of rarefaction curves of biodiversity. The residual standard error of the curve

186 fitting is defined as follows:

$$187 \quad R_{se} = \sqrt{\frac{1}{n-p} \sum_{i=1}^n R_i^2} \quad (2)$$

188 where n and p denote the number of data points and fitting coefficients ($p = 2$ in this study),
189 respectively; $n - p$ represents degrees of freedom; and R_i is the residual of the i th data
190 point. Thus, R_{se} indicates the average distance of the data points from the fitted curve,
191 which can be interpreted as the goodness of fit of the curve. Although there is no certain
192 criterion for R_{se} , an excessively large R_{se} (i.e. > 1) implies that the assumption of the
193 methodology may be violated. Therefore, application of the method should be reconsidered
194 in such cases.

195

196 5. Estimation of Ichnodiversity

197 Next, the ichnotaxa coverage parameter is defined. This parameter describes
198 completeness of sampled diversity. Here, the slope of the tangential lines of Equation 1 at
199 any given L (S_L) is calculated as follows:

$$200 \quad S_L = \frac{a_1 a_2}{1 + a_2 L} \quad (3)$$

201 Chao and Jost (2012) argued that the sample coverage (C) can be estimated as follows:

$$202 \quad C = 1 - S_L \quad (4)$$

203 The sample coverage (C) becomes 1 when sampled diversity is equivalent to the real
204 diversity, and thus the slope of the rarefaction curve is zero, and is expected to be positive
205 because the parameter C is the proportion of the total number of individuals in the

206 hypothetical population. However, the slope of the curve of Equation 1 (S_L) is not always
 207 less than 1, so that C may be negative when Equation 4 is used. Therefore, the slope S_L is
 208 normalized by the slope of Equation 1 at $L = 0$ (S_0):

$$209 \quad \overline{S}_L = \frac{S_L}{a_1 a_2} \quad (5)$$

210 For the biodiversity rarefaction curve, the number of taxa always becomes one when the
 211 first specimen is sampled, and thus the slope of the discretized biodiversity rarefaction
 212 curve is 1 at the interval where the number of samples is from 0 to 1. Because of the
 213 normalization represented by Equation 5, the normalized slope of Equation 1 becomes 1 at
 214 $L = 0$. Here the ichnotaxa coverage parameter \overline{C} is defined as follows:

$$215 \quad \overline{C} = 1 - \overline{S}_L \quad (6)$$

216 The parameter \overline{C} becomes the minimum value 0 when $L = 0$, and converges to 1 as L
 217 increases. Equation 6 can be recalculated as:

$$218 \quad \overline{C} = \frac{a_2 L}{1 + a_2 L} \quad (7)$$

219 Equation 1 is recalculated as follows, with the aid of Equation 7:

$$220 \quad E_s = a_1 \ln \left(1 + \frac{\overline{C}}{1 - \overline{C}} \right) \quad (8)$$

221 Equation 8 indicates that the ratio of E_s between two samples at any given \overline{C} is always
 222 constant. Consequently, fluctuation of the ichnodiversity in the outcrop image data at any
 223 given ichnotaxa coverage parameter is obtained independent of differences in the exposed

224 area of outcrops.

225

226 VERIFICATION OF METHODOLOGY

227 The method proposed in this study was applied to artificial data of
228 ichnoassemblages to verify the methodology, specifically the effects of distribution patterns
229 of ichnofossils on bedding planes and shortage of outcrop exposure area. Four artificial
230 outcrop images were produced with different distribution patterns and various types of
231 ichnofossils. In addition, incomplete outcrop images were also produced by gradually
232 decreasing the area of these four outcrop images. Then, the ichnodiversity estimated from
233 the artificial images was compared with the true values for methodology verification.

234

235 Artificial Data

236 Artificial ichnofossil images were allocated on virtual bedding planes to generate
237 artificial outcrop images showing ichnoassemblages. Chance of occurrence of each
238 ichnotaxon was set to the prescribed value (Fig. 2). In this series of experiments, two types
239 of spatial distribution patterns of ichnofossils were examined: uniform and patchy
240 distributions. In addition, two types of maximum number of ichnotaxa were also examined
241 (10 and 5 ichnotaxa) (Fig. 3). The procedures of allocating the ichnofossil images were as
242 follows: (1) 150 ichnofossil images were chosen based on their chance of occurrence (Fig.
243 2). (2) Ichnofossil images were allocated onto a white colored image (6000×4500 pixels).
244 The coordinates of each ichnofossil image were determined by the following equation:

245
$$p_p = \left(\frac{d_{\min}}{D} \right)^{2k} \quad (9)$$

246 where p_p denotes the probability of whether an ichnofossil image is allocated at a point
247 (p) that was chosen by a uniform random number; D is a specific distance from the point
248 p ($D = 200$ pixels in this study); d_{\min} is the minimum value of the distances between p and
249 other points the ichnofossil images were already allocated; and k is a coefficient that
250 determines the distribution pattern of the ichnofossil images ($k = -1, 1$). When $k = 1$, the
251 point p that is far from other points in which the ichnofossil images were already allocated
252 tends to be adopted, and thus the distribution pattern becomes uniform. In contrast, when
253 $k = -1$, the point p that is close to other points tends to be adopted so that the ichnofossil
254 images are allocated in proximity with each other and the patchy distribution pattern is
255 established. Resolution of each image was set at 50 pixels/cm, thus, the maximum area of
256 the outcrop images was $10,800 \text{ cm}^2$. All ichnofossil images were 100×100 pixels (2×2
257 cm).

258 These outcrop images were then partially and progressively covered by black
259 coloration to produce images of the reduced areas, which were analyzed in order to verify
260 the effects on areas with outcrop exposure.

261

262 Results

263 Results of the image-resampling method are summarized in Fig. 4. After 100
264 repetitions of the resampling process, the mean number of observed ichnotaxa (\overline{N}_{is})

265 against each length of the resampling line (L) was estimated. The 95% confidence intervals
266 for each \overline{N}_{is} were calculated by bootstrapping, replicating 10,000 times, with normal
267 approximation. Confidence intervals of the estimated numbers of ichnotaxa were larger in
268 patchy distribution patterns than in uniform distribution patterns. For all distribution
269 patterns, the estimated numbers of ichnotaxa increased as the lengths of resampling lines
270 increased, and they approached their maximum numbers of ichnotaxa when the resampling
271 lines filled the whole outcrop images. As a whole, the relationship between the lengths of
272 resampling lines and the estimated number of ichnotaxa were well-fitted to the function
273 expressed in Equation 1. Parameters of curve fitting are summarized in Table 1.

274 As a result of analyses, the fitting coefficients a_1 and a_2 were estimated as
275 follows, respectively: 1.726 and 0.036 in the uniform distribution with 10 ichnotaxa; 0.835
276 and 0.047 in the uniform distribution with 5 ichnotaxa; 1.797 and 0.029 in the patchy
277 distribution with 10 ichnotaxa; and 0.900 and 0.031 in the patchy distribution with 5
278 ichnotaxa (Table 1). Using these values, the coverage parameters (\overline{C}) were calculated. The
279 relationships between the coverage parameters (\overline{C}) and the expected numbers of ichnotaxa
280 (E_s) are shown in Fig. 5. The shapes of curves, which were based on data of equivalent
281 maximum number of ichnotaxa, were similar to each other. Ratios of E_s among artificial
282 data are shown in Table 2.

283 The results of the numerical experiments for reduced outcrop exposure are shown
284 in Figure 6 and Table 1. The shapes of the \overline{C} -based ichnofossil rarefaction curves were
285 well maintained if the exposure area decreased, especially in diverse artificial data (uniform

286 and patchy distribution patterns with 10 ichnotaxa) (Fig. 6A, C). In contrast, the E_s in the
287 case with 5 ichnotaxa tended to be under- or overestimated when the total exposure area
288 was smaller than 50% of the original image (Fig. 6B, D; Table 1).

289

290

APPLICATION TO FIELD DATA

291

292

293

294

295

296

Geological Setting

297

298

299

300

301

302

303

304

305

306

307

The MIDIRT method was applied to the field data measured in deposits of the submarine channel-levee complex in the Oligocene Izaki Olistolith of the Nichinan Group (Sakai et al. 1987). The variation of ichnodiversity in the channel-fill deposit and the levee deposit was evaluated with MIDIRT.

The Oligocene to lower Miocene Nichinan Group is distributed on the southeastern part of Kyushu, southwestern Japan (Fig. 7). The Nichinan Group is composed of various sized coherent blocks and intensely deformed beds. They are interpreted as the deposits of the olistostrome which was caused by gravitational instability from the restart of subduction of the Philippine Sea plate in 21–17 Ma (Sakai 1988a, 1988b, 1988c). The Izaki Olistolith distributed in Izaki-bana is considered as one of the coherent blocks that were originally deposited in the deep-sea setting (Sakai et al. 1987) (Fig. 7). It is mainly composed of alternating beds of turbidite sandstone and mudstone and is interpreted to be a deposit of a submarine channel-levee complex (Yumi and Ishihara 2012). The Izaki Olistolith can be divided into three stratigraphic units based on lithology. The lower and upper parts of the Izaki Olistolith (units A and C; Fig. 7D) are comprised of thin-bedded

308 turbidite sandstone and mudstone beds. The sandstone beds in the units A and C are mainly
309 1–20 cm thick, and climbing ripple and convolute lamination are observable. The mudstone
310 beds are 10–20 cm thick. Taking this into consideration, the deposits of the units A and C
311 are interpreted as submarine levee deposits (Arnott 2010). In contrast, the middle part of the
312 Izaki Olistolith (unit B; Fig. 7D) consists of thick-bedded turbidite sandstones and
313 thin-bedded mudstones. The thickness of the sandstone beds in the unit B ranges from 5 to
314 200 cm. The current ripple, climbing ripple, convolute lamination, and parallel lamination
315 are observable on the top of sandstone beds. The sole marks, such as flute cast or groove
316 cast, are commonly found on the bottom surface of thick-bedded (more than 100 cm thick)
317 sandstone beds. The mudstone beds in the middle part are less than 10 cm thick. The
318 alternating beds in the unit B show an upward-thinning succession. These characteristics
319 indicate that the unit B of the Izaki Olistolith is the submarine channel-fill deposit (Arnott
320 2010).

321

322 Ichnoassemblage of the Izaki Olistolith

323 The ichnoassemblage in the Izaki Olistolith is mainly composed of graphoglyptids
324 (Fig. 8). This study investigated the number of ichnogenera and measured the exposed area
325 of the bottom surfaces of each turbidite sandstone bed. For the image-resampling method,
326 photographs of the bottom surfaces of sandstone beds were obtained through field work,
327 and then were colored appropriately for each ichnogenus. We observed 5,960 cm² and
328 33,520 cm² of bottom surfaces of the turbidite sandstone beds in the levee deposit and the
329 channel-fill deposit, respectively.

330 A total of 11 ichnogenera were recognized on the sole surface of sandstone beds in
331 the levee deposit (Table 3). Abundant *Phycosiphon incertum* and *Gordia marina* are
332 characteristics of this deposit. Graphoglyptids, such as *Megagraption irregulare* or
333 *Paleodictyon strozzii*, were rarely observed in relatively thin-bedded sandstones (5–15 cm
334 thick). In contrast, the thick-bedded sandstones (50–200 cm thick) contain fewer
335 ichnogenera even though the bottom surfaces of these beds are widely exposed.

336 A total of 22 ichnogenera were found on the sole surface of sandstone beds in the
337 channel-fill deposit (Table 3). Various types of graphoglyptids were observed in these
338 deposits. *Helminthorhapse japonica* and *Paleodictyon strozzii* were common.
339 *Desmograption inversum*, *Punctorhapse parallela*, and *Spirorhapse involuta* are rarely
340 observed. Thick-bedded sandstones in the lower part of the channel-fill deposits (unit B1;
341 Fig. 7D) yielded fewer ichnogenera, whereas various ichnogenera occurred in the upper
342 part (unit B2; Fig. 7D).

343

344 Results

345 Results of our image-resampling method are summarized in Fig. 9. As with the
346 artificial data, the numbers of ichnogenera in each sedimentary environment increased as
347 observed area increased. The plots were well-fitted to Equation 1. The residual standard
348 error (R_{se}) was 0.180 in the channel-fill deposit and 0.300 in the levee deposit (Table 4).

349 The fitting coefficients a_1 and a_2 in the channel-fill deposit were 4.916 and
350 0.003, respectively. In contrast, those in the levee deposit were 2.825 and 0.007,
351 respectively (Table 4). Using these values, the coverage parameters (\bar{C}) were calculated.

352 The relationship between the coverage parameters (\bar{C}) and the expected numbers of
353 ichnotaxa (E_s) were then estimated (Fig. 10). E_s , when $\bar{C} = 0.8$ in the channel-fill and
354 levee deposits was 7.913 and 4.547, respectively. Therefore, the ichnodiversity in the
355 channel-fill deposit was 1.740 times higher than in the levee deposit.

356

357 DISCUSSION

358

Selection of the Fitting Function

359

360

361

362

363

364

365

366

367

368

369

370

371

372

This study employed Equation 1 as the fitting function of the rarefaction curves, according to Mauffrey et al. (2007). Mauffrey et al. (2007) used and evaluated three models, which included the Exponential Dependence model (recast to Equation 1), Clench model, and Linear Dependence model, to fit the individual-based rarefaction curves for species richness extrapolation of the small-mammal communities in a French Guianan rainforest. They concluded that Equation 1 was the most suitable for extrapolation of the rarefaction curves because the estimated diversity based on Equation 1 showed the most similar value to the known local biodiversity in their study area based on previous trapping missions, although goodness of fit for these three models was not significantly different. In contrast, van Rooijen (2009) estimated snake species richness of the Santubong Peninsula in Borneo by extrapolating the individual-based rarefaction curve. He applied two exponential models to fit the rarefaction curve, the negative exponential and Weibull functions. The Weibull function was recast as the following equation:

$$Y = A(1 - \exp(b - ct)) \quad (10)$$

373 where Y denotes the expected number of species; A is total number of species; t is sample
374 size; and b and c are constants that denote the ease which species are found. van Rooijen
375 (2009) argued that the Weibull function exhibited higher goodness of fit than the negative
376 exponential function, and expected species richness based on the Weibull function
377 corresponded with the value estimated by the Chao I estimator (Chao 1984). Therefore, he
378 concluded that the Weibull function is suitable for extrapolation of the rarefaction curve.

379 For ichnodiversity, there are some problems in fitting the Weibull function to the
380 relationship between L and E_s . First, goodness of fit of the Weibull function is lower than
381 that of Equation 1. The Akaike's Information Criterion (AIC) for the uniform distribution
382 with 10 ichnotaxa was 24.44 when fitted to the Weibull function, whereas 1.38 when fitted
383 to Equation 1. Figure 11 shows the result of fitting the Weibull function for uniform
384 distribution with 10 ichnotaxa. The fitted Weibull function tended to overestimate when L
385 was an intermediate value (approximately 4,000 to 5,000 cm) and underestimate when L
386 was small or large (Fig. 11). Second, the asymptote of the Weibull function ($Y = A$) strongly
387 depended on the observed maximum number of ichnotaxa. The maximum number of
388 ichnotaxa estimated by the fitted Weibull function was 9.701 for 100% exposed artificial
389 data of the uniform distribution with 10 ichnotaxa. In contrast, it was 8.224 in for 50%
390 exposed data in which exactly 8 ichnotaxa were observed. Therefore, estimation using the
391 Weibull function is unsuitable to correct outcrop exposure bias.

392 Application of Equation 1 leads an infinite value of ichnodiversity when $L \rightarrow \infty$
393 or $\bar{C} = 1$ because Equation 1 does not have an asymptote (eq. 1 and 8). This implies that
394 ichnodiversity in the hypothetical population cannot be estimated by extrapolation of

395 Equation 1. However, E_s standardized by \bar{C} in the interpolation interval can be
396 compared fairly, regardless of the difference in distribution pattern and outcrop exposure
397 bias (see below for discussion). Furthermore, the ratio of E_s among any two datasets was
398 always constant at any given \bar{C} (eq. 8). Taking this into consideration, Equation 1 is valid
399 as the fitting function for the relationship between L and E_s , if the analysis aim is
400 comparison of E_s in the interpolation interval and not extrapolation.

401

402 Validity of the Method

403 Verification of the method by applying artificial outcrop image data indicated that
404 the MIDIRT is a valuable method to evaluate ichnodiversity regardless of outcrop exposure
405 area, the total number of ichnotaxa, or distribution patterns of ichnofossils on the bedding
406 planes. Each \bar{C} -based fitting curve of artificial data corresponded to another curve which
407 had an equal maximum number of ichnotaxa (Fig. 5). As the \bar{C} -based fitting curves are the
408 logarithmic functions passing an origin (eq. 8), ratios of E_s in each artificial image are
409 constant even if E_s is normalized at any ichnotaxa coverage parameter. For example, the
410 ratio of E_s in the uniform distribution pattern with 10 ichnotaxa and uniform distribution
411 pattern with 5 ichnotaxa was constantly 2.067 (Table 2). In contrast, the ratio of the
412 maximum numbers of ichnotaxa in these conditions was 2.000. Therefore, it was
413 considered that the ratio of E_s was reflected in the maximum numbers of ichnotaxa in
414 each condition. In other combinations of conditions, the ratio of E_s also showed the same

415 tendency (Table 2). The \bar{C} -based fitting curves showed that E_s obtained from the images
416 showing patchy distribution patterns with 10 ichnotaxa were slightly overestimated when
417 compared with E_s in conditions with equivalent maximum number of ichnotaxa (Fig. 5;
418 Table 2). The increasing rate of observed number of ichnotaxa (a_2) in the patchy
419 distribution with 10 ichnotaxa was smaller than that of other conditions (Table 1). This was
420 likely due to a larger area of bedding plane in which no ichnotaxa were observed, and thus,
421 \bar{C} at a given L was also smaller. This may have led to the overestimation of E_s in the
422 patchy distribution with 10 ichnotaxa. However, differences between the ratios of E_s and
423 that of the maximum numbers of ichnotaxa were small enough to disregard. These results
424 indicate that ichnodiversity can be compared fairly, independent of outcrop exposure bias
425 using MIDIRT.

426

427

Application to outcrops

428

429

430

431

432

433

434

435

We tested our methodology to the outcrops of the channel-levee system in the
Izaki Olistolith, and suggested that the effect of outcrop exposure bias cannot be ignored.
The result of our method shows that the ratio of E_s in the channel-fill deposit and levee
deposit is 1.740 although that of the raw numbers of ichnotaxa is higher value (2.000). In
the case of the Izaki Olistolith, the channel-fill deposits expose better than the levee
deposits, which leads to the apparently larger ichnodiversity. The decrease in the ratio of
the ichnodiversity indicates that, therefore, our method corrected this bias.

In general, however, it is estimated that the ichnodiversity in channel-fill deposits

458 the effect of observation bias. Wetzel (1991) suggested that pore water oxygenation level
459 and benthic food content strongly affect ichnodiversity. Cummings and Hodgson (2011)
460 argued that fluctuation in number of ichnotaxa in submarine fan deposits of the Basque
461 Basin, northern Spain was induced by dysoxic/anoxic conditions. In addition, biodiversity
462 of benthic communities can be affected by benthic food content on the seafloor. For
463 instance, it is well known that biodiversity increases are associated with decreasing organic
464 matter input, whereas biodiversity decreases in oversupplied organic matter conditions (P-R
465 model; Pearson and Rosenberg 1978). However, ichnodiversity does not directly
466 correspond with benthic biodiversity (Buatois and Mángano 2013), so that further
467 examination is needed for understanding relationship between benthic food content and the
468 resultant variation in ichnodiversity.

469 Although there are some issues and room for development, the MIDIRT method is
470 applicable for both characterizing depositional facies and temporal variations of
471 ichnodiversity. There have been attempts to construct the model for estimation of
472 paleoenvironmental conditions based on fluctuation of ichnodiversity (e.g. Heard and
473 Pickering 2008; Cummings and Hodgson 2011; Phillips et al. 2011; Callow et al. 2013).
474 These models will be more reliable with fair comparison of ichnodiversity by the MIDIRT
475 method.

476

477

CONCLUSIONS

478 We proposed a new method, MIDIRT, to evaluate ichnodiversity from outcrop
479 records. Although the number of ichnotaxa is generally affected by outcrop exposure bias,

480 existing methods to correct sample size bias cannot be applied to ichnofossil analyses as the
481 relative abundance of ichnofossils is difficult to measure because of the variations in
482 morphological characteristics. The method we proposed corrects this bias by using an
483 image-resampling technique combined with the SQS method (Alroy 2010b, 2010c). The
484 method was verified by applying it to four types of artificial data. As a result, the ratio of
485 the estimated sample ichnodiversity approximated the ratio of the real ichnodiversity with
486 each dataset. Results also suggested that ichnodiversity can be compared fairly, regardless
487 of area of outcrop exposure and distribution patterns of ichnofossils on the bedding planes.
488 The method was also applied to field data of the ichnoassemblage in the channel-levee
489 complex of the Oligocene Izaki Olistolith of the Nichinan Group. The result of the analysis
490 indicated that ichnodiversity, independent of outcrop exposure bias, was higher in the
491 channel-fill deposit than the levee deposit. In contrast, previous studies showed an inverse
492 trend of increasing ichnodiversity from channel-axial to marginal environments. Evaluation
493 of ichnodiversity by the MIDIRT method is expected to be useful in reconstructing
494 paleoenvironmental conditions.

495

496 ACKNOWLEDGEMENTS

497 Takao Ubukata (Kyoto University) provided useful comments on statistics and
498 body fossil diversity. The paper benefited from constructive reviews by two anonymous
499 referees, as well as from numerous editorial comments by M. Gabriela Mángano. A part of
500 this study was supported by a grant from the Fukada Geological Institute (2014). All these
501 contributions are gratefully acknowledged.

502

503

REFERENCES

504 ALROY, J., 2010a, The shifting balance of diversity among major marine animal groups:

505 Science, v. 329, p. 1191–1194, doi: 10.1126/science.1189910.

506 ALROY, J., 2010b, Geographical, environmental and intrinsic biotic controls on Phanerozoic

507 marine diversification: Paleontology, v. 53, p. 1211–1235, doi:

508 10.1111/j.1475-4983.2010.01011.x.

509 ALROY, J., 2010c, Fair sampling of taxonomic richness and unbiased estimation of

510 origination and extinction rates, *in* J. Alroy and G. Hunt (eds.), Quantitative Methods

511 in Paleobiology: The Paleontological Society, Boulder, p. 55–80.

512 ARNOTT, R.W.C., 2010, Deep-marine sediments and sedimentary system, *in* N.P. James and

513 R.W. Dalrymple (eds.), Facies Models 4, Geological Association of Canada, St. John's,

514 NL, Canada, p. 295–322.

515 BAYET-GOLL, A., NETO DE CARVALHO, C., MAHMUDY-GHARAEI, M.H., AND NADAF, R.,

516 2015, Ichnology and sedimentology of a shallow marine Upper Cretaceous

517 depositional system (Neyzar Formation, Kopet-Dagh, Iran): palaeoceanographic

518 influence on ichnodiversity: Cretaceous Research, v. 56, p. 628–646, doi:

519 10.1016/j.cretres.2015.07.008.

520 BROMLEY, R.G. AND EKDALE, A. A., 1984, *Chondrites*: a trace fossil indicator of anoxia in

521 sediments: Science, v. 224, p. 872–875, doi: 10.1126/science.224.4651.872.

522 BUATOIS, L.A. and MÁNGANO, M.G., 2013, Ichnodiversity and ichnodisparity: significance

523 and caveats: Lethaia, v. 46, p. 281–292, doi: 10.1111/let.12018.

- 524 BUATOIS, L.A., MANGANO, M.G., AND MAPLES, C.G., 1997, The paradox of nonmarine
525 ichnofaunas in tidal rhythmites; intergrating sedimentologic and ichnologic data from
526 the Late Cretaceous of eastern Kansas, USA: *PALAIOS*, v. 12, p. 467–481, doi:
527 10.2307/3515384.
- 528 BUATOIS, L.A., MANGANO, M.G., OLEA, R.A., and WILSON, M.A., 2016, Decoupled
529 evolution of soft and hard substrate communities during the Cambrian Explosion and
530 Great Ordovician Biodiversification Event: *Proceedings of the National Academy of*
531 *Sciences*, v. 113, p. 6945–6948, doi: 10.1073/pnas.1523087113.
- 532 CALLOW, H.T.R., KNELLER, B., DYKSTRA, M., and MCLLOY, D., 2014, Physical, biological,
533 geochemical and sedimentological controls on the ichnology of submarine canyon and
534 slope channel systems: *Marine and Petroleum Geology*, v. 54, p. 144–166, doi:
535 10.1016/j.marpetgeo.2014.02.016.
- 536 CALLOW, H.T.R., MCLLOY, D., KNELLER, B., and DYKSTRA, M., 2013, Integrated
537 ichnological and sedimentological analysis of a Late Cretaceous submarine
538 channel-levee system: the Rosario Formation, Baja California, Mexico: *Marine and*
539 *Petroleum Geology*, v. 41, p. 277–294, doi: 10.1016/j.marpetgeo.2012.02.001.
- 540 CHAO, A. and JOST, L., 2012, Coverage-based rarefaction and extrapolation: standardizing
541 samples by completeness rather than size: *Ecology*, v. 93, p. 2533–2547, doi:
542 10.1890/11-1952.1.
- 543 CHAO, A., 1984, Nonparametric estimation of the number of classes in a population:
544 *Scandinavian Journal of Statistics*, v. 11, p. 265–270, doi: 10.2307/4615964.
- 545 CUMMINGS, J.P. and HODGSON, D.M., 2011, Assessing controls on the distribution of

546 ichnotaxa in submarine fan environments, the Basque Basin, Northern Spain:
547 *Sedimentary Geology*, v. 239, p. 162–187, doi: 10.1016/j.sedgeo.2011.06.009.

548 GIANNETTI, A. AND MCCANN, T., 2010, The upper Paleocene of the Zumaya section
549 (northern Spain): review of the ichnological content and preliminary palaeoecological
550 interpretation: *Ichnos*, v. 17, p. 137–161, doi: 10.1080/10420941003659550.

551 GINGRAS, M.K., MACEACHERN, J.A., AND DASHTGARD, S.E., 2011, Process ichnology and
552 the elucidation of physico-chemical stress: *Sedimentary Geology*, v. 237, p. 115–134,
553 doi: 10.1016/j.sedgeo.2011.02.006.

554 GOOD, I.J., 1953, The population frequencies of species and the estimation of population
555 parameters: *Biometrika*, v. 40, p. 237–264, doi: 10.1093/biomet/40.3-4.237.

556 HAUCK, T., DASHTGARD, S.E., PEMBERTON, S.G., AND GINGRAS, M.K., 2009,
557 Brackish-water ichnological trends in a microtidal barrier island–embayment system,
558 Kouchibouguac National Park, New Brunswick, Canada: *PALAIOS*, v. 24, p. 478–496,
559 doi: 10.2110/palo.2008.p08-056r.

560 HEARD, T.G. and PICKERING, K.T., 2008, Trace fossils as diagnostic indicators of
561 deep-marine environments, middle Eocene Ainsa-Jaca basin, Spanish Pyrenees:
562 *Sedimentology*, v. 55, p. 809–844, doi: 10.1111/j.1365-3091.2007.00922.x.

563 HEARD, T.G., PICKERING, K.T., and CLARK, J.D., 2014, Ichnofabric characterization of a
564 deep-marine clastic system: a subsurface study of the middle Eocene Ainsa System,
565 Spanish, Pyrenees: *Sedimentology*, v. 61, p. 1298–1331, doi: 10.1111/sed.12101.

566 HURLBERT, S.H., 1971, The nonconcept of species diversity; a critique alternative
567 parameters: *Ecology*, v. 52, p. 577–586, doi: 10.2307/1934145.

568 HYLAND, J., BALTHIS, L., KARAKASSIS, I., MAGNI, P., PETROV, A., SHINE, J., VESTERGAARD,
569 O., AND WARWICK, R., 2005, Organic carbon content of sediments as an indicator of
570 stress in the marine benthos: *Marine Ecology Progress Series*, v. 295, p. 91–103, doi:
571 10.3354/meps295091.

572 KNAUST, D., 2007, Invertebrate trace fossils and ichnodiversity in shallow-marine
573 carbonates of the German Middle Triassic (Muschelkalk), *in* R.G. Bromley, L.A.
574 Buatois, M.G. Mángano, J.F. Genise, and R.N. Melchor (eds.), *Sediment-Organism*
575 *Interactions: A Multifaceted Ichnology: SEPM Special Publication*, v. 88. p. 221–238.

576 KNAUST, D., WARCHOL, M., AND KANE, I.A., 2014, Ichnodiversity and ichnoabundance:
577 revealing depositional trends in a confined turbidite system: *Sedimentology*, v. 61, p.
578 2218–2267, doi: 10.1111/sed.12134.

579 MAUFFREY, J. F., STEINER, C. AND CATZEFLIS, F. M., 2007, Small-mammal diversity and
580 abundance in a French Guianan rain forest: test of sampling procedures using species
581 rarefaction curves: *Journal of Tropical Ecology*, v. 23, p. 419–425, doi:
582 10.1017/S0266467407004154.

583 ORR, P. J., 2001, Colonization of the deep-marine environment during the early
584 Phanerozoic: the ichnofaunal record: *Geological Journal*, v. 36, p. 265–278, doi:
585 10.1002/gj.891.

586 PEARSON, T.H. AND ROSENBERG, R., 1978, Macrobenthic succession in relation to organic
587 enrichment and pollution of the marine environment: *Oceanography and Marine*
588 *Biology: An Annual Review*, v. 16, p. 229–311.

589 PHILLIPS, C., MCILROY, D., and ELLIOTT, T., 2011, Ichnological characterization of

590 Eocene/Oligocene turbidites from the Grès d'Annot Basin, French Alps, SE France:
591 Palaeogeography, Palaeoclimatology, Palaeoecology, v. 300, p. 67–83, doi:
592 10.1016/j.palaeo.2010.12.011.

593 SAKAI, H., 1988a, Toi-misaki olistostrome of the southern belt of the Shimanto Terrane,
594 south Kyushu—I. Reconstruction of depositional environments and stratigraphy
595 before collapse: Journal of Geological Society of Japan, v. 94, p. 733–747, doi:
596 10.5575/geosoc.94.733. (In Japanese).

597 SAKAI, H., 1988b, Toi-misaki olistostrome of the southern belt of the Shimanto Terrane,
598 south Kyushu—II. Deformation structure of huge submarine slides and processes of
599 formation: Journal of Geological Society of Japan, v. 94, p. 837–853 doi:
600 10.5575/geosoc.94.837. (In Japanese).

601 SAKAI, H., 1988c, Origin of the Misaki Olistostrome Belt and re-examination of the
602 Takachiho Orogeny: Journal of Geological Society of Japan, v. 94, p. 945–961 doi:
603 10.5575/geosoc.94.945. (In Japanese).

604 SAKAI, T., KUSABA, T., NISHI, H., KOMORI, M., and WATANABE, M., 1987, Olistostorome of
605 the Shimanto Terrane in the Nichinan area, southern part of the Miyazaki Prefecture,
606 south Kyushu—with reference to deformation and mechanism of emplacement of
607 olistolith: Science Reports, Department of Geology, Kyushu University, v. 15, p. 167–
608 199. (In Japanese).

609 SANDERS, H.L., 1968, Marine benthic diversity: a comparative study: The American
610 Naturalist, v. 102, p. 243–282, doi: 10.1086/282541.

611 TIMMER, E.R., BOTTERILL, S.E., GINGRAS, M.K., AND ZONNEVELD, J.-P., 2016, Visualizing a

612 process ichnology dataset, Lower Cretaceous McMurray Formation, NE Alberta,
613 Canada: Bulletin of Canadian Petroleum Geology, v. 64, p. 251–265, doi:
614 10.2113/gscpgbull.64.2.251.

615 UCHMAN, A., 2003, Trends in diversity, frequency and complexity of graphoglyptid trace
616 fossils: evolutionary and palaeoenvironmental aspects: Palaeogeography,
617 Palaeoclimatology, Palaeoecology, v. 192, p. 123–142, doi:
618 10.1016/S0031-0182(02)00682-X.

619 VAN ROOIJEN, J., 2009, Estimating the snake species richness of the Santubong Peninsula
620 (Borneo) in two different ways: Contributions to Zoology, v. 78, p. 141–147.

621 WETZEL, A., 1991, Ecologic interpretation of deep-sea trace fossil communities:
622 Palaeogeography, Palaeoclimatology, Palaeoecology, v. 85, p. 47–69, doi:
623 10.1016/0031-0182(91)90025-M.

624 WETZEL, A., AND UCHMAN, A., 1998, Deep-sea benthic food content recorded by
625 ichnofabrics; a conceptual model based on observations from Paleogene flysch,
626 Carpathians, Poland: Palaios, v. 13, p. 533–546, doi: 10.2307/3515345.

627 YUMI, M. AND ISHIHARA, Y., 2012, Characterization of erosional marks in the base of
628 sediment-gravity-flow deposits: special reference to the effect of flow duration for
629 flute mark formation: Journal of Sedimentological Society of Japan, v. 71 p. 173–190,
630 doi: 10.4096/jssj.71.173.

631

632 Figure and Table Captions

633 FIG. 1.—Schematic diagram of Measurement of Ichnofossil Diversity by

634 Image-Resampling Technique (MIDIRT) procedures. The procedures are as follows:
635 (1) outcrop images containing trace fossils are acquired; (2) each identified ichnotaxon
636 is illustrated with a particular gray scale value in outcrop images; (3a) one of the
637 outcrop images is selected at random, and (3b) the line of interest that has a given
638 length L is randomly set in the image. Then the number of types of gray scale values
639 are counted along the line of interest; (3c) the processes of resampling (3a, b) are
640 repeated 100 times, and the results are averaged for obtaining an expected number of
641 ichnotaxa corresponding to the length of resampling line L . (4) The relationship
642 between length of the line-of-interest (approximated to observed area) L and
643 expected number of ichnotaxa E_s is estimated by repeating processes (3a–c) with
644 changing sampling length L ; and (5) the coverage parameter, which is an estimate of
645 the ratio of a measured value to actual diversity, is calculated from the slope of the
646 tangential lines of the curve. See details of these procedures in the text.

647 FIG. 2.—List of illustrated symbols of ichnofossils and their chance of occurrence.

648 FIG. 3.—Four artificial outcrop images that were generated for verification of the MIDIRT
649 method proposed in this study. **A)** Uniform distribution pattern with 10 ichnotaxa. **B)**
650 Uniform distribution pattern with 5 ichnotaxa. **C)** Patchy distribution pattern with 10
651 ichnotaxa. **D)** Patchy distribution pattern with 5 ichnotaxa.

652 FIG. 4.—Relationships between resampling length and number of detected ichnotaxa, based
653 on analysis of artificial outcrop images by MIDIRT. Each plot represents the average
654 number of detected ichnotaxa that was obtained from 100 trials using the given
655 resampling length. The fitted curves and coefficients of determination are also shown.

656 Error bars indicate the 95% confidence intervals of the average numbers of detected
657 ichnogenera. **A)** Result from the image of uniform distribution pattern with 10
658 ichnotaxa. **B)** Result from the image of uniform distribution pattern with 5 ichnotaxa.
659 **C)** Result from the image of patchy distribution pattern with 10 ichnotaxa. **D)** Result
660 from the image of patchy distribution pattern with 5 ichnotaxa.

661 FIG. 5.—Expected number of ichnotaxa E_s against the ichnotaxa coverage parameter used
662 in the MIDIRT method. Shapes of fitted curves for E_s only depend on the actual
663 number of ichnotaxon, and are independent of spatial patterns of ichnofossil
664 distribution.

665 FIG. 6.— \bar{C} -based fitting curves of the artificial outcrop images showing the effect of
666 outcrop exposure bias based on the result of MIDIRT analysis. **A)** Uniform
667 distribution pattern with 10 ichnotaxa. **B)** Uniform distribution pattern with 5
668 ichnotaxa. **C)** Patchy distribution pattern with 10 ichnotaxa. **D)** Patchy distribution
669 pattern with 5 ichnotaxa.

670 FIG. 7.—Maps showing the study area. **A)** Location of study area. **B)** Geological map of the
671 southern part of the Nichinan coastal area, southern part of Kyushu, southwest Japan.
672 Modified after Sakai (1988c). **C)** Lithological map of the Izaki-bana. In addition to
673 coherent alternating beds of turbidite sandstone and mudstone, intensely deformed
674 slumped beds are widely distributed on the Izaki-bana. Various ichnofossils that
675 mainly comprised graphoglyptids are observable at the basal surfaces of turbidite beds.
676 **D)** Schematic columnar section of the Izaki Olistolith. Stratigraphic intervals and
677 interpretation of depositional environment are also shown. st: siltstone, vfs: very fine

678 sandstone, fs: fine sandstone, ms: medium sandstone.

679 FIG. 8.—Ichnofossils occurring on the bottom surface of sandstone beds in the Izaki
680 Olistolith. **A)** *Cosmorhapse parva*. **B)** *Gordia marina*. **C)** *Helminthorhapse japonica*.
681 **D)** *Paleodictyon minimum* (*Pm*) and *P. strozzii* (*Ps*). **E)** *Punctorhapse parallela*. **F)**
682 *Spirophycus bicornis*. Scale bar = 2 cm.

683 FIG. 9.—Relationships between resampling lengths and number of ichnogenera obtained by
684 the MIDIRT method applied to field data from the Izaki Olistolith. Each plot
685 represents the average number of detected ichnogenera of 100 trials for each
686 resampling length. The fitted curves and coefficients of determination are also shown.
687 Error bars indicate the 95% confidence intervals of the average numbers of observed
688 ichnogenera. **A)** Channel-fill deposits. **B)** Levee deposits.

689 FIG. 10.—Variation of expected number of ichnotaxa E_s of the channel-fill deposits and
690 the levee deposits in the Izaki Olistolith against the ichnotaxa coverage parameter.

691 FIG. 11.—Comparison of two fitting functions with the artificial data of the uniform
692 distribution with 10 ichnotaxa.

693 TABLE. 1.—Coefficients of the curves fitted to the resampled data of the artificial outcrop
694 images, parameters showing goodness of fit, and ratio of ichnodiversity. The rightmost
695 column represents ratios between ichnodiversity of each exposure condition and 100%
696 exposed data in the same distribution patterns and maximum numbers of ichnotaxa.

697 TABLE. 2.—Results comprising ratios of estimated numbers of ichnotaxa for artificial
698 outcrop images.

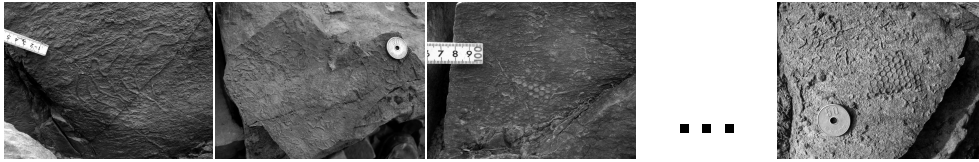
699 TABLE. 3.—List of ichnotaxa occurring on the bottom of sandstone beds in the Izaki

700 Olistolith.

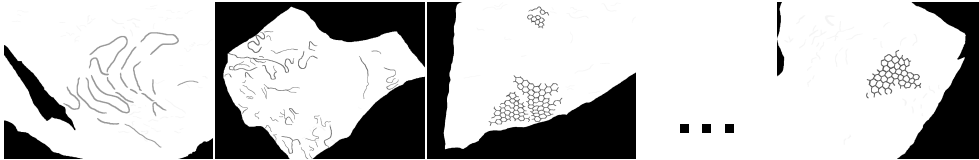
701 TABLE. 4.—Coefficients of the curves fitted to the resampled data of the field data of the

702 Izaki Olistolith and parameters showing goodness of fit.

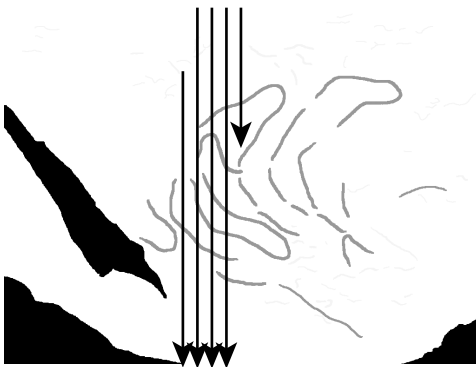
1. Acquisition of outcrop images



↓ 2. Painting with particular gray scale for each ichnotaxon

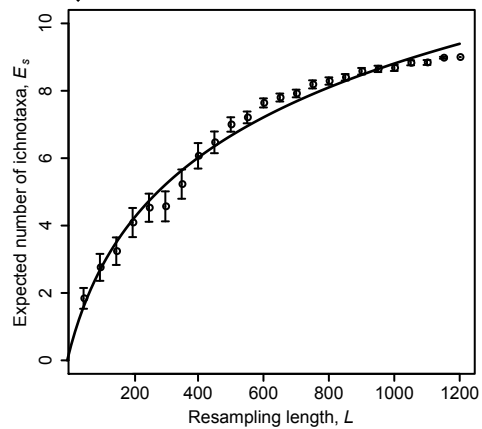


↓ 3a. Selecting a image at random ↑ 3c. Repeating 100 times



3b. Counting kinds of gray scale value on the line-of-interest randomly set

↓ 4. Curve fitting to resampled data



5. Estimation of ichnodiversity

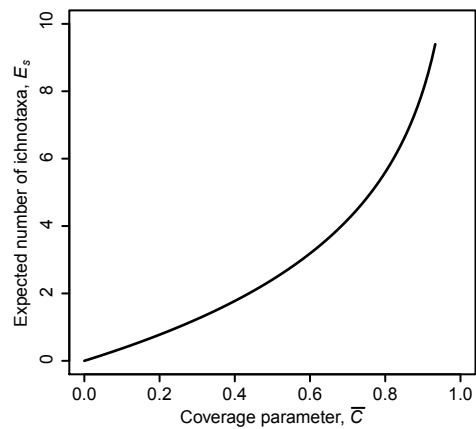


Fig. 1

Ichnofossil images	Chances of occurrence	
	High diversity	Low diversity
<i>A</i> 	0.30	0.64
<i>B</i> 	0.20	0.23
<i>C</i> 	0.20	0.09
<i>D</i> 	0.10	0.03
<i>E</i> 	0.06	0.01
<i>F</i> 	0.05	-
<i>G</i> 	0.03	-
<i>H</i> 	0.03	-
<i>I</i> 	0.02	-
<i>J</i> 	0.01	-

Fig. 2

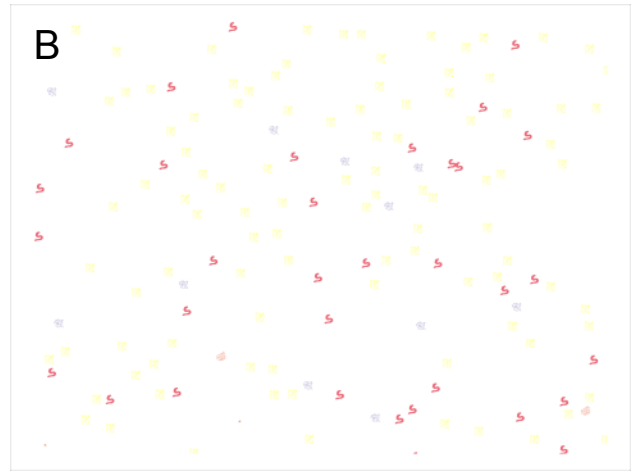


Fig. 3

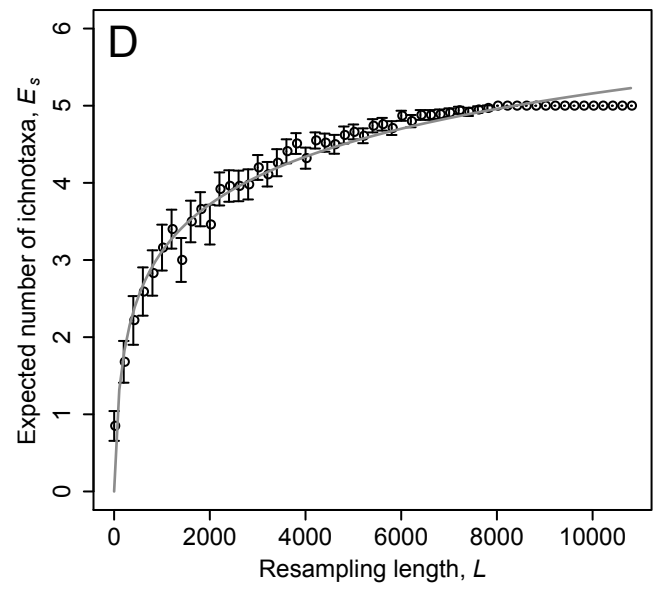
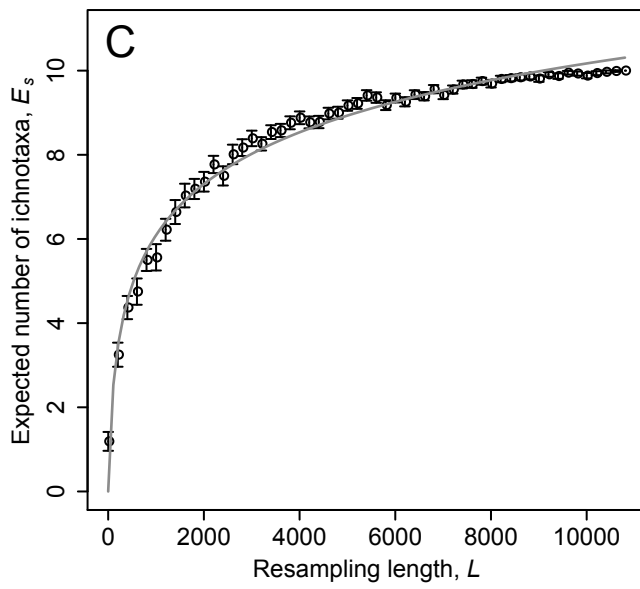
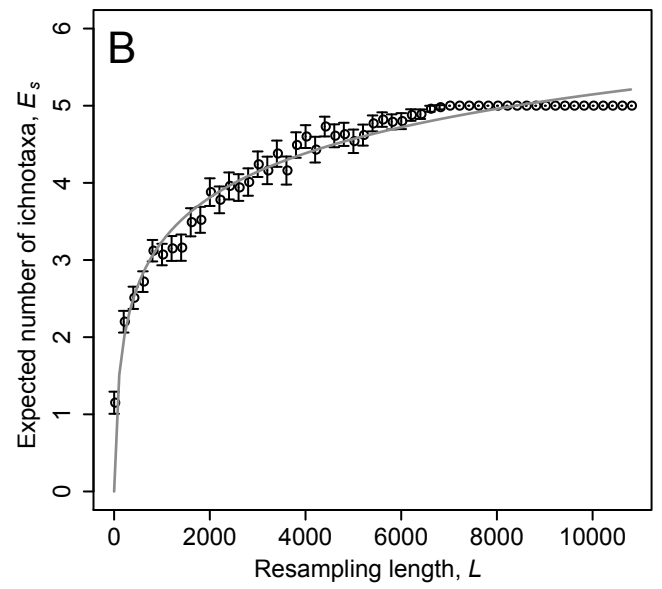
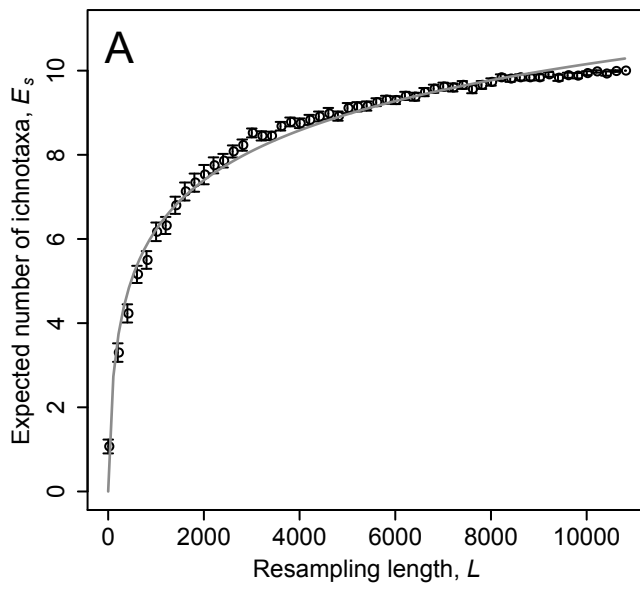


Fig. 4

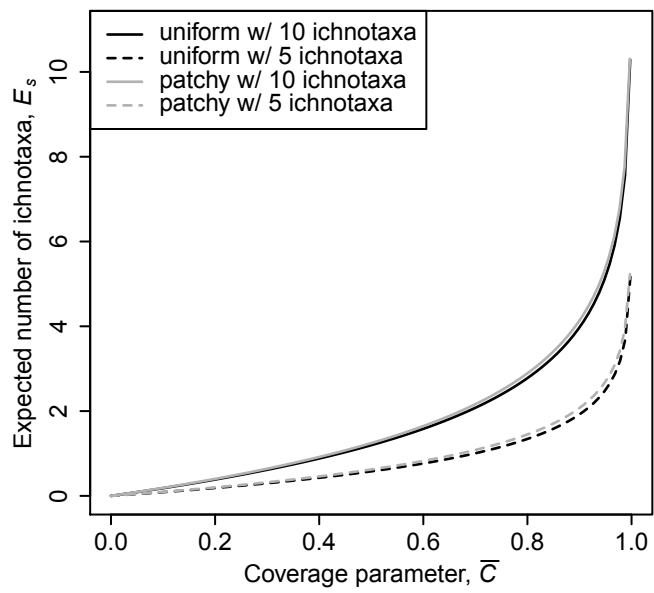


Fig. 5

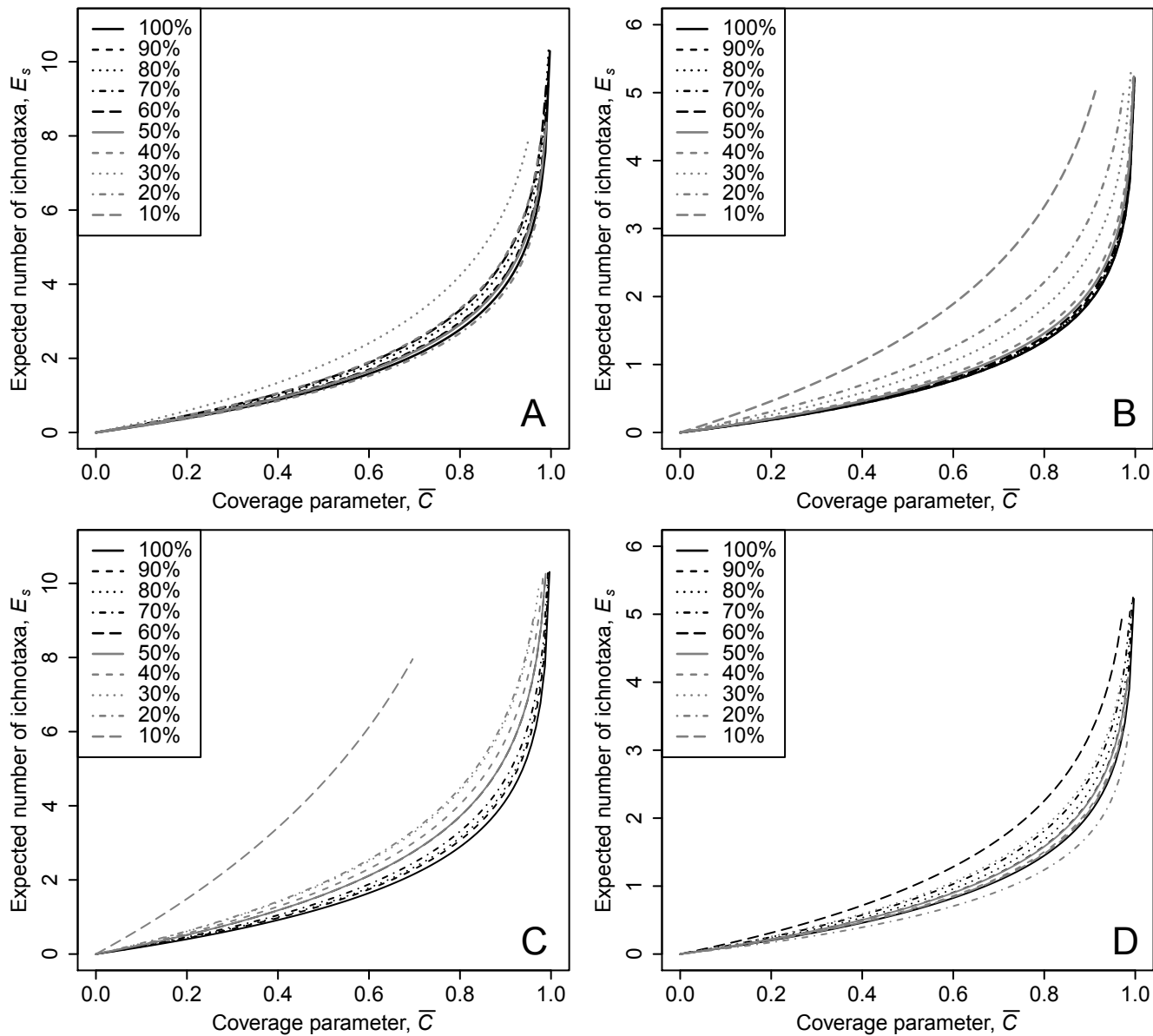


Fig. 6

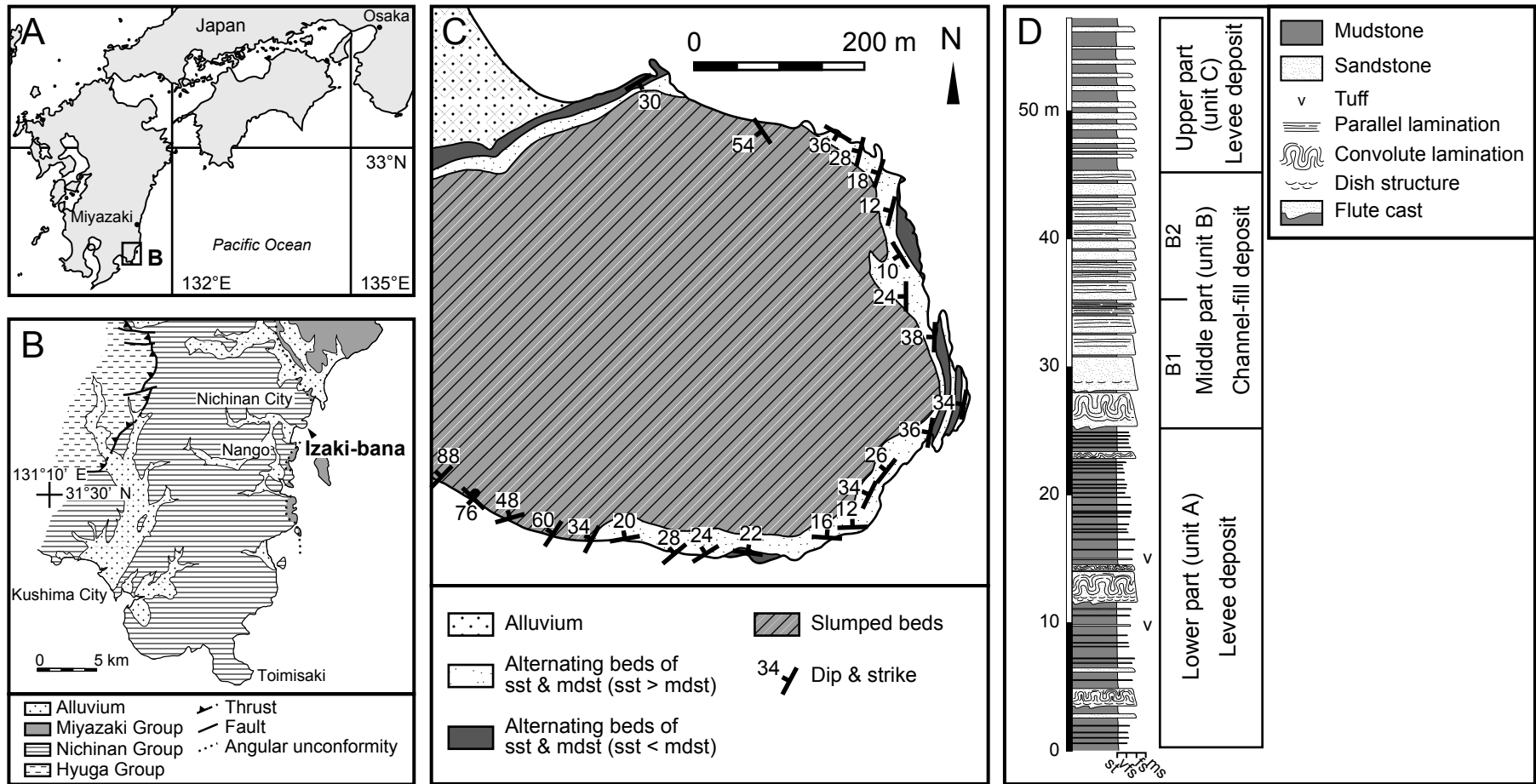


Fig. 7

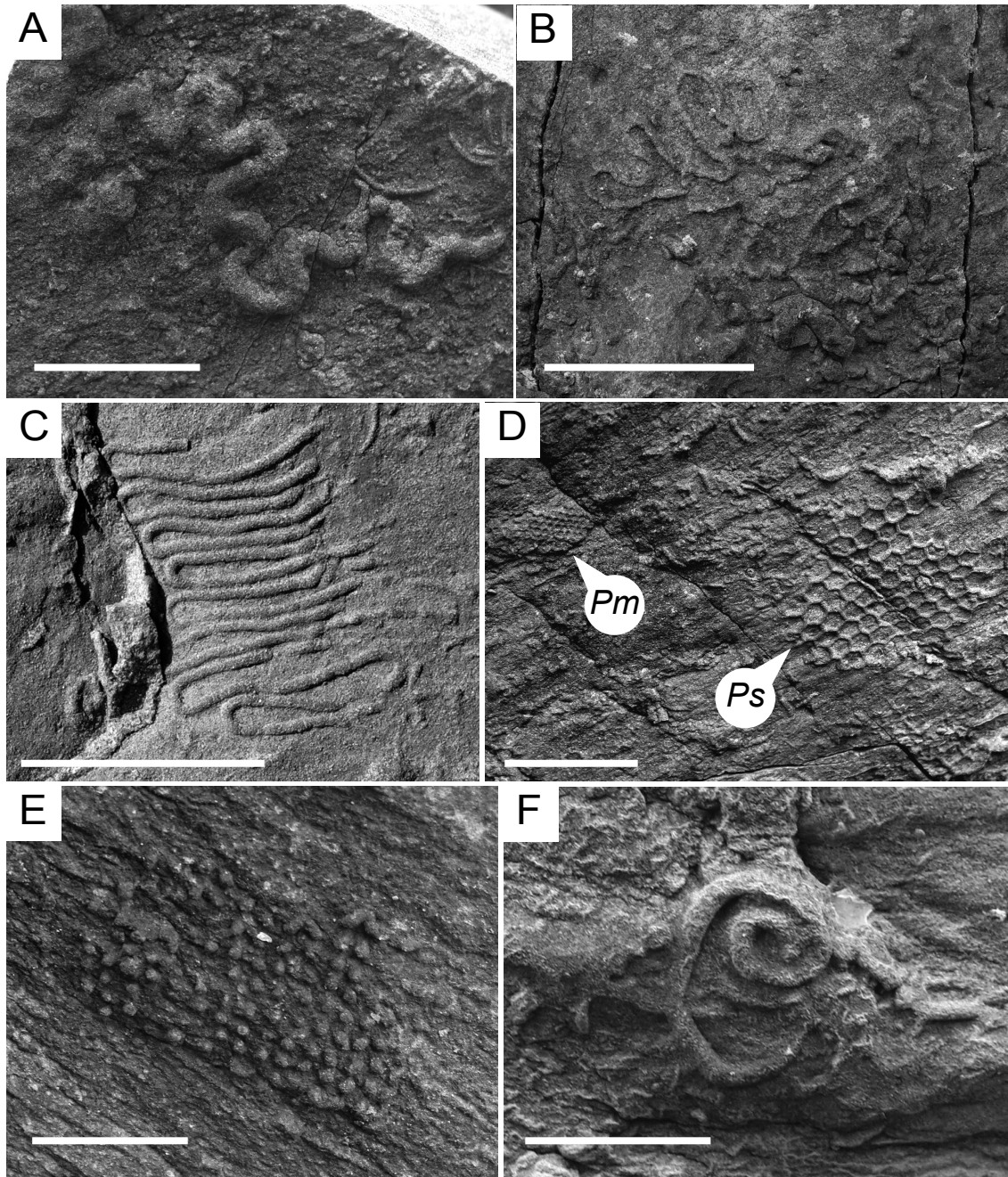


Fig. 8

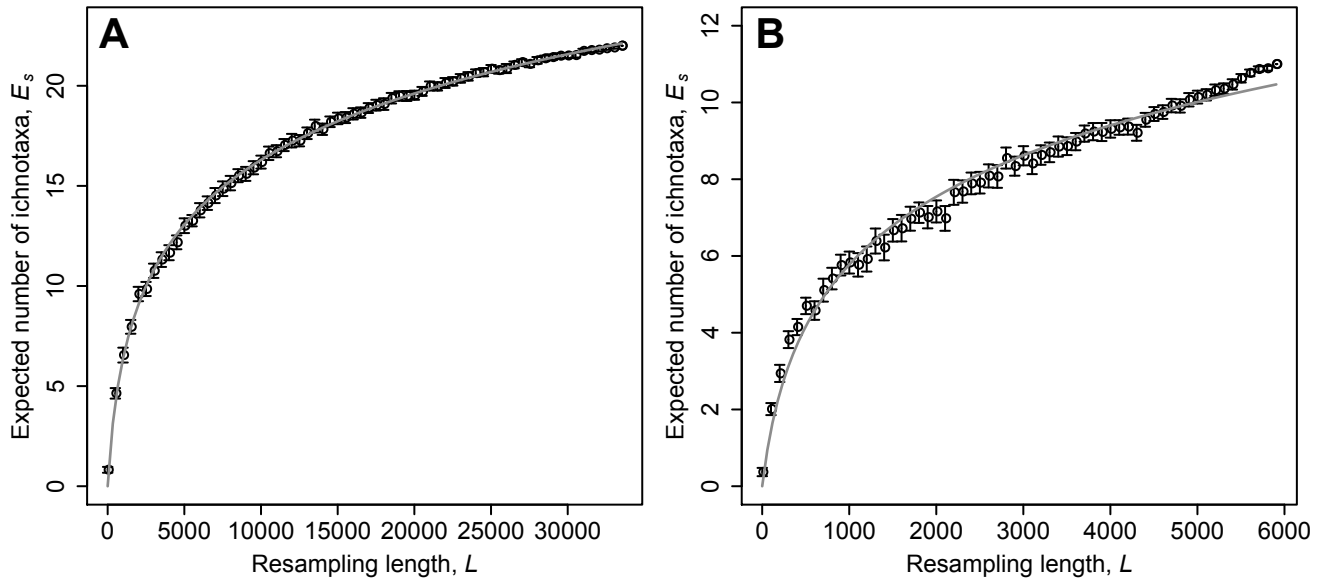


Fig. 9

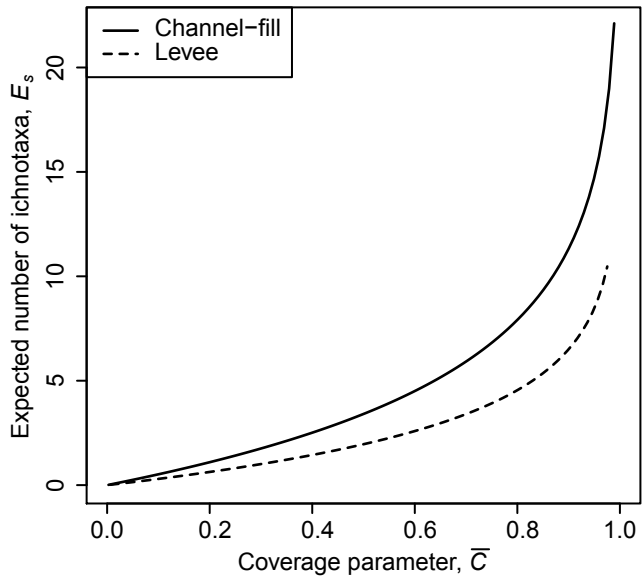


Fig. 10

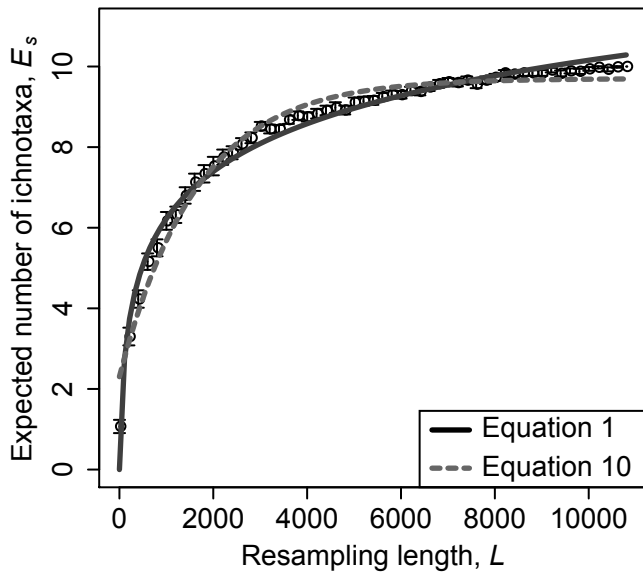


Fig. 11

Distribution patterns	Exposure	a_1			a_2			R_{se}	Ratio
		Estimate	Std. Error	p	Estimate	Std. Error	p		
uniform w/ 10 ichnotaxa	100%	1.726	0.041	1.440E-42	0.036	0.004	4.960E-11	0.236	-
	90%	1.847	0.049	3.700E-22	0.026	0.003	7.010E-08	0.178	1.070
	80%	1.966	0.065	5.890E-20	0.022	0.003	9.820E-07	0.230	1.139
	70%	1.837	0.073	2.730E-18	0.022	0.004	8.690E-06	0.252	1.065
	60%	2.051	0.068	5.490E-20	0.015	0.002	1.010E-07	0.216	1.188
	50%	1.812	0.061	6.910E-20	0.018	0.002	1.330E-07	0.194	1.050
	40%	2.073	0.029	2.060E-28	0.011	0.001	1.480E-16	0.078	1.201
	30%	2.628	0.107	4.990E-18	0.006	0.001	3.820E-09	0.203	1.523
	20%	1.667	0.044	2.700E-22	0.017	0.001	2.340E-11	0.109	0.966
	10%	1.811	0.069	1.190E-18	0.013	0.001	2.280E-10	0.112	1.049
uniform w/ 5 ichnotaxa	100%	0.835	0.035	2.630E-30	0.047	0.011	4.250E-05	0.205	-
	90%	0.836	0.033	1.960E-18	0.052	0.011	9.990E-05	0.124	1.001
	80%	0.853	0.030	2.010E-19	0.051	0.009	2.060E-05	0.114	1.022
	70%	0.857	0.034	2.140E-18	0.058	0.012	7.690E-05	0.127	1.027
	60%	0.878	0.037	9.380E-18	0.059	0.013	1.290E-04	0.138	1.052
	50%	0.907	0.041	4.950E-17	0.060	0.014	2.085E-04	0.151	1.086
	40%	0.954	0.048	6.080E-16	0.058	0.014	4.191E-04	0.174	1.143
	30%	1.144	0.062	3.060E-15	0.031	0.007	1.306E-04	0.200	1.371
	20%	1.374	0.037	3.770E-22	0.017	0.001	2.720E-11	0.090	1.646
	10%	2.064	0.047	1.300E-23	0.010	0.001	1.450E-15	0.066	2.472
patchy w/ 10 ichnotaxa	100%	1.797	0.046	1.380E-40	0.029	0.004	2.030E-10	0.263	-
	90%	1.906	0.065	1.140E-19	0.023	0.004	2.530E-06	0.234	1.061
	80%	1.949	0.072	5.990E-19	0.023	0.004	5.380E-06	0.254	1.085
	70%	2.056	0.085	6.910E-18	0.020	0.004	1.200E-05	0.290	1.144
	60%	2.307	0.072	1.500E-20	0.013	0.002	2.220E-08	0.223	1.284
	50%	2.310	0.076	4.790E-20	0.016	0.002	5.390E-08	0.235	1.286
	40%	2.510	0.069	6.690E-22	0.014	0.001	4.060E-10	0.195	1.397
	30%	2.735	0.050	7.580E-26	0.011	0.001	1.200E-14	0.124	1.523
	20%	2.783	0.083	5.660E-21	0.012	0.001	4.970E-11	0.181	1.549
	10%	6.682	0.255	1.300E-18	0.002	0.000	1.830E-14	0.101	3.719
patchy w/ 5 ichnotaxa	100%	0.900	0.030	2.890E-35	0.031	0.005	1.360E-07	0.169	-
	90%	0.989	0.043	1.900E-17	0.021	0.004	4.340E-05	0.151	1.098
	80%	1.046	0.048	8.100E-17	0.017	0.003	4.730E-05	0.164	1.162
	70%	1.124	0.018	6.260E-27	0.012	0.001	1.020E-13	0.058	1.249
	60%	1.401	0.034	4.710E-23	0.005	0.000	2.580E-12	0.081	1.556
	50%	0.983	0.050	8.270E-16	0.011	0.002	1.570E-05	0.145	1.092
	40%	0.934	0.034	3.650E-19	0.018	0.002	1.690E-07	0.102	1.038
	30%	1.159	0.065	5.900E-15	0.010	0.002	7.610E-06	0.156	1.288
	20%	0.770	0.074	3.490E-10	0.032	0.011	9.245E-03	0.218	0.855
	10%	0.918	0.098	2.450E-09	0.032	0.011	6.280E-03	0.237	1.019

Table 1

	uniform w/ 10 ichnotaxa	uniform w/ 5 ichnotaxa	patchy w/ 10 ichnotaxa	patchy w/ 5 ichnotaxa
uniform w/ 10 ichnotaxa	-	0.484	1.041	0.522
uniform w/ 5 ichnotaxa	2.067	-	2.152	1.078
patchy w/ 10 ichnotaxa	0.961	0.465	-	0.501
patchy w/ 5 ichnotaxa	1.917	0.927	1.996	-

Table 2

Sedimentary environments	Ichnotaxa	
Levee (11 ichnogenera 12 ichnospecies)	<i>Bergaueria</i> isp.	
	<i>Gordia marina</i>	
	<i>Gordia</i> isp.	
	<i>Helminthopsis abeli</i>	
	<i>Megagraption irregulare</i>	
	<i>Nereites missouriensis</i>	
	<i>Paleodictyon strozzii</i>	
	<i>Paleophycus</i> isp.	
	<i>Phycosiphon incertum</i>	
	<i>Spirorhapse involuta</i>	
	Circular trace	
	Radial trace	
	Channel-fill (22 ichnogenera 24 ichnospecies)	<i>Asteriacites lumbricalis</i>
		<i>Belorhapse zickzack</i>
<i>Bergaueria</i> isp.		
<i>Cosmorhapse parva</i>		
<i>Desmograption ichtyforme</i>		
<i>Gordia marina</i>		
<i>Gordia</i> isp.		
<i>Halopoa imbriata</i>		
<i>Helminthopsis abeli</i>		
<i>Helminthorhapse japonica</i>		
<i>Lorenzina</i> isp.		
<i>Mammilichnis aggeris</i>		
<i>Megagraption irregulare</i>		
<i>Nereites missouriensis</i>		
<i>Paleodictyon minimum</i>		
<i>Paleodictyon strozzii</i>		
<i>Paleophycus</i> isp.		
<i>Phycosiphon incertum</i>		
<i>Punctorhapse parallela</i>		
<i>Spirophycus bicornis</i>		
<i>Spirorhapse involuta</i>		
Bloom like trace		
Circular trace		
Radial trace		

Table 3

	a_1			a_2			R_{se}
	Estimate	Std. Error	p	Estimate	Std. Error	p	
Channel-fill	4.916	0.035	6.994E-85	2.650.E-03	7.171.E-05	2.733E-46	0.180
Levee	2.825	0.077	2.050E-42	6.722.E-03	5.841.E-04	1.030E-16	0.300

Table 4